Atmos. Chem. Phys. Discuss., 7, 9053–9092, 2007
www.atmos-chem-phys-discuss.net/7/9053/2007/

Atmospheric Chemistry and Physics Discussions

Secondary organic aerosol in the global aerosol – chemistry transport model Oslo CTM2

C. R. Hoyle, T. Berntsen, G. Myhre, and I. S. A. Isaksen

Department of Geosciences, University of Oslo, Norway

Received: 15 June 2007 – Accepted: 15 June 2007 – Published: 26 June 2007

Correspondence to: C. R. Hoyle (c.r.hoyle@geo.uio.no)

Abstract

The global chemical transport model Oslo CTM2 has been extended to include the formation, transport and deposition of secondary organic aerosol (SOA). Precursor hydrocarbons which are oxidised to form condensible species include both biogenic species such as terpenes and isoprene, as well as species emitted predominantly by anthropogenic activities (toluene, m-xylene, methylbenzene and other aromatics). A model simulation for 2004 gives an annual global SOA production of approximately 55 Tg. Of this total, 2.5 Tg is found to consist of the oxidation products of anthropogenically emitted hydrocarbons, and about 15 Tg is formed by the oxidation products of isoprene. The global production of SOA is increased to about 76 Tg yr^{-1} by allowing semi-volatile species to condense on ammonium sulphate aerosol. This brings modelled organic aerosol values closer to those observed, however observations in Europe remain significantly underestimated, raising the possibility of an unaccounted for SOA source. Allowing SOA to form on ammonium sulphate aerosol increases the contribution of anthropogenic SOA from about 4.5% to almost 9% of the total production. The importance of NO_3 as an oxidant of SOA precursors is found to vary regionally, causing up to 50%–60% of the total amount of SOA near the surface in polluted regions and less than 25% in more remote areas. This study underscores the need for SOA to be represented in a more realistic way in global aerosol models in order to better reproduce observations of organic aerosol burdens in industrialised and biomass burning regions.

1 Introduction

The study of atmospheric aerosol is important for many reasons, ranging from its impact on human health, to its influences on atmospheric chemistry and climate.

Organic matter makes up a significant portion of the global aerosol burden, accounting for around 20–50% of total fine aerosol mass at continental mid latitudes, with a

ACPD

7, 9053–9092, 2007

contribution of up to 90% in tropical forested areas (Kanakidou et al., 2005). This organic aerosol can be emitted directly into the atmosphere through processes such as biomass or fossil fuel burning, and aerosol emitted in this manner is termed primary organic aerosol (POA). In addition, organic species that are emitted as volatile gases (VOC) may undergo oxidation reactions to form substances with lower vapour pressures, which subsequently condense to form secondary organic aerosol (SOA).

While black carbon (BC) aerosol absorbs solar radiation and generally leads to a warming of the Earth's atmosphere (Haywood and Shine, 1995; Penner et al., 1998; Schulz et al., 2006), the direct radiative effect of organic carbon (OC) aerosol is negative (Liousse et al., 1996; Cooke et al., 1999; Schulz et al., 2006). In addition to the direct effect on the Earth's radiation balance, carbonaceous aerosols can influence the formation, lifetime and radiative properties of clouds. This may occur through aerosol either causing a modification in the temperature profile of the atmosphere (Hansen et al., 1997; Ackerman et al., 2000), or serving as CCN and directly influencing the number and size of cloud particles as well as the lifetimes of clouds (Twomey, 1959, 1977; Albrecht, 1989).

Apart from the climatic effects of SOA, effects upon human health may also be significant as particulate matter is known to exacerbate respiratory illnesses and generally increase mortality (Ostro and Chestnut, 1998; Jones, 1999).

Under certain conditions, SOA may form the majority of the organic aerosol (Tsigaridis and Kanakidou, 2003; Pun et al., 2003; Zhang et al., 2005; Volkamer et al., 2006; Robinson et al., 2007), therefore an accurate representation in global models is necessary if these are to be used to calculate the climatic effects of organic aerosol. The inclusion of SOA is also important for comparisons of modelled aerosol optical depth with that measured from satellites, and the evaluation of the models representation of spatial and temporal variations in the optical depth. The inclusion of SOA in the Oslo CTM2 completes the set of major aerosol components in the model.

Several modelling studies have given estimates of the global burden and distribution of SOA from predominantly natural precursors (Chung and Seinfeld, 2002; Tsigaridis

and Kanakidou, 2003; Griffin et al., 1999a; Derwent et al., 2003; Henze and Seinfeld, 2006).

Some classes of compounds included in anthropogenic emissions are capable of forming SOA upon oxidation in the atmosphere. These include toluene, xylene and trimethylbenzenes. The contribution of these species to global SOA budgets has been evaluated by a recent study (Tsigaridis et al., 2005), and found to be a minor fraction (8%) of the contribution from naturally emitted precursors. Kanakidou et al. (2000) evaluated the anthropogenic effect on the concentrations of oxidants in the troposphere, and found that increases in tropospheric oxidants have lead to a factor of three to four increase in SOA production via O_3 oxidation of biogenic precursor gases, between pre-industrial times and the present. They also found that an increase in anthropogenic POA had lead to greater SOA production.

In previous modelling studies it has been suggested that SOA formation as a result of hydrocarbon oxidation by NO_3 is very minor in comparison to that by ozone and the hydroxyl radical (Chung and Seinfeld, 2002; Tsigaridis and Kanakidou, 2003), however the results of some measurement campaigns show oxidation of VOC by the nitrate radical may be significant (Brown et al., 2005; Vrekoussis et al., 2004; Allan et al., 2002; Penkett et al., 1993).

As the Oslo CTM2 has not been used for detailed studies of SOA previously, the chemical scheme has been updated to account for the necessary processes. The SOA scheme used in this study is based upon that of Chung and Seinfeld (2002), however, it has been extended to include several new species. The results presented here provide a new estimate of the global SOA production and burden and are an important contribution towards reducing the uncertainty in the global SOA production and burden figures.

In the next section, a very brief description of the Oslo CTM2 will be provided, and the newly implemented SOA code will be described in some detail. The model experiment and results will be described in Sect. 3, and the contribution of NO_3 oxidation to global and regional SOA formation will be discussed in Sect. 4. A summary and conclusions

will be presented in Sect. 5.

2 Model description

2.1 The Oslo CTM2

The Oslo CTM2 is a three dimensional off-line chemistry transport model, which was run with T42 (approximately 2.8°×2.8°) horizontal resolution for this study. The model includes 40 layers between the surface and 10 hPa. The meteorological data used was generated by running the Integrated Forecast System (IFS) of the European Centre for Medium Range Weather Forecasts (ECMWF), for the year 2004, and was updated (offline) in the CTM every 3 h. The chemical time step in the troposphere is 15 min, in the free troposphere the transport time step is 1 h, in the boundary layer it is 15 min. In the configuration used in this study, the model includes 122 gas and condensed phase chemical species, all of which are transported. The chemistry scheme accounts for the most important parts of the ozone-NO_x-hydrocarbon chemistry cycle. For the chemistry calculations, the QSSA chemistry solver (Hesstvedt et al., 1977) is used.

Emissions of CO (1121.8 Tg(CO) yr^{-1}), NO_x (44.3 Tg(N) yr^{-1}) and non-methane hydrocarbons are taken from the Precursors of Ozone and their Effects in the Troposphere (POET) inventory (Granier et al., 2005).

More detailed descriptions of the model, as well as validation against measurements can be found in Berntsen and Isaksen (1997); Brunner et al. (2003); Berglen et al. (2004); Isaksen et al. (2005); Schulz et al. (2006) and Myhre et al. (2007).

2.2 Biogenic VOC emissions

Emissions of monoterpenes and Other Reactive Volatile Organic Compounds (ORVOC) are listed in Table 2 and are from the Global Emissions Inventory Activity (GEIA) data base. They are representitive of 1990 (Guenther et al., 1995). The uncertainties

ACPD
7, 9053–9092, 2007

EGU

associated with these emissions are estimated as being between a factor of 3 (Guenther et al., 1995) and a factor of 5 (Kanakidou et al., 2005). The emitted species are assigned to 12 tracers using global contribution factors from Griffin et al. (1999a) (see Table 1). The use of a single factor, globally, for the contribution of a particular species to the regional monoterpene or ORVOC emissions is justifiable as the contribution factors do not vary greatly with location (Kanakidou et al., 2005).

The 12 tracers are subsequently grouped into 5 classes, combining species which form oxidation products with similar aerosol forming properties (Chung and Seinfeld, 2002).

Emissions of isoprene are from the POET inventory (Granier et al., 2005), however they are scaled down to 220 $\mathrm{Tg\,yr^{-1}}$ (IPCC, 2001). This is rather low compared to the range of likely global isoprene emissions (250–750 $\mathrm{Tg\,yr^{-1}}$) given in Kanakidou et al. (2005), as well as other recent estimates (Lathière et al., 2006; Guenther et al., 2006), therefore the SOA contribution from the oxidation products of isoprene may be underestimated slightly. In the model, the total monthly emissions of monoterpenes and isoprene are distributed throughout the month, with emissions at a particular location and time depending on temperature and light. The emissions of monoterpenes have been previously modelled by an equation which does not take into account a light dependence (Guenther et al., 1995), however, recently a number of studies have shown that monoterpene emissions from many types of vegetation do in fact exibit a strong dependence on light, with negligable emissions taking place during the hours of darkness (Kesselmeier and Staudt, 1999; Kuhn et al., 2002; Moukhtar et al., 2005; Dindorf et al., 2006).

Here we apply the equation given by Guenther et al. (1995) to represent isoprene emissions, to scale both isoprene and monoterpene emissions:

$$C_T = \frac{\exp\left[\frac{C_{T1}(T-T_S)}{RT_sT}\right]}{1+\exp\left[\frac{C_{T2}(T-T_M)}{RT_ST}\right]} \quad (1)$$

The temperature dependence of the emissions is given by C_T and R is the gas constant (8.314 J K^{-1} mol^{-1}). The remaining variables are empirical coefficients (C_{T1} = 95,000 J mol^{-1}, C_{T2}=230 000 J mol^{-1} and T_M=314 K) (Guenther et al., 1995). In order to limit the monoterpene and isoprene emissions to the day time, the solar elevation angle was calculated according to Holtslag and Ulden (1983) for all model grid points at the Earth's surface, with a time resolution of one hour, and emissions were switched off when the sun was below the horizon. When the sun was above the horizon, emissions were scaled using Eq. (1). During the polar night, no emission scaling was carried out, so that any (very small) emissions in these areas contained in the data files would be included. The total monthly isoprene or monoterpene emissions at a particular grid point are unchanged by this temperature and light scaling.

2.3 Anthropogenic VOC emissions

Emissions of toluene, m-xylene, trimethylbenzene, as well as the lumped species "other aromatic species", are from the emissions inventories produced in the RETRO (REanalysis of the TROpospheric chemical composition over the past 40 years) project Schultz et al. (2007)[1], for the year 2000. The total global emissions from these species are listed in Table 2. The seasonal dependence of the sources is taken into account in the RETRO inventory. In the Oslo CTM2, emissions of "other aromatic species" are added to the toluene tracer, and trimethylbenzene is added to the m-xylene tracer.

2.4 Representation of POA

POA can serve as a surface for the condensation of SOA (Kanakidou et al., 2005) and the mass of SOA in the model therefore depends partly upon the mass of POA. The treatment of POA in the Oslo CTM2 is similar to that described by Cooke et al. (1999).

[1] Schultz, M. G., Pulles, T., Brand, R., van het Bolscher, M., and Dalsren, S. B.: A global data set of anthropogenic CO, NOx, and NMVOC emissions for 1960–2000, in preparation, 2007.

Emissions of OC from fossil fuel combustion are from the inventory of Bond et al. (2004) and are representative of 1996. Total fossil fuel and biofuel combustion OC emissions are about 8.8 Tg(C) yr^{-1}, with approximately a factor of two uncertainty (Bond et al., 2004). Emissions of OC from biomass burning (21.5 Tg yr^{-1} in total) are taken from the Global Fire Emissions Database version 2 (GFEDv2), for 2004 (van der Werf et al., 2006). POA is transported in four variables, according to source (biomass or fossil fuel burning) and solubility. The hydrophobic part is assumed to be insoluble, while the hydrophilic part is completely soluble, and subject to wet removal by convective events and large scale rain. For the conversion of hydrophobic OC to hydrophilic OC, a conversion rate of 21% day^{-1} is used (Maria et al., 2004).

2.5 Formation of SOA

Precursor hydrocarbons are transported in the model, and undergo gas phase oxidation via reaction with either O_3, OH or NO_3. The rate constants for the oxidation of monoterpenes and ORVOC are shown in Table 3, oxidation rates for the m-xylene and toluene tracers as well as isoprene are shown in Table 4. A two product model (see Hoffmann et al., 1997) is used to represent the oxidation products of the precursor hydrocarbons and their aerosol forming properties, whereby the mass based stoichiometric coefficients (α) and equilibrium gas-particle partitioning coefficients (K) are empirical values determined from chamber studies (Hoffmann et al., 1997). The values of the stoichiometric coefficients for product k of the reaction of hydrocarbon i and oxidant j, $\alpha_{i,j,k}$ are given in Table 5. The reaction products of oxidation via OH and O_3 are considered together, and as the NO_3 oxidation rate of $\beta-$Pinene is used to represent NO_3 oxidation of all class I–class V hydrocarbons, only one product is necessary in this case (Chung and Seinfeld, 2002; Griffin et al., 1999b).

The partitioning between the gas and aerosol phases is calculated assuming equilibrium and using the partitioning coefficients $K_{i,j,k}$, listed in Table (6). Under the assumption that the activity coefficient of each compound is constant, in the organic aerosol

phase, the temperature dependence of the partitioning coefficients is given by:

$$\frac{K_{i,j,k}(T)}{K_{i,j,k}(T_r)} = \frac{T}{T_r} \exp\left[\frac{\Delta H_{i,j,k}}{R}\left(\frac{1}{T} - \frac{1}{T_r}\right)\right] \quad (2)$$

where T_r is a reference temperature, T is the temperature of interest, R is the gas constant and $\Delta H_{i,j,k}$ is the enthalpy of vaporisation. In this study, we use ΔH=42 kJ mol^{-1} for all SOA (Henze and Seinfeld, 2006; Chung and Seinfeld, 2002).

The concentration of each of the oxidation products in the gas phase is given by:

$$[G]_{i,j,k} = \frac{[A]_{i,j,k}}{K_{i,j,k} M_o} \quad (3)$$

where $[G]_{i,j,k}$ is the gas phase product concentration, $[A]_{i,j,k}$ is the condensed phase product concentration and M_o is the total mass of organic aerosol (i.e. the sum of POA and SOA). Using Eq. (4), M_o is calculated iteratively,

$$\sum_{i,j,k}\left[\frac{K_{i,j,k}(T)([A]^0_{i,j,k} + [G]^0_{i,j,k})}{(1 + K_{i,j,k}(T)M_o)}\right] + \frac{[POA]}{M_o} = 1 \quad (4)$$

from the initial gas and aerosol phase concentrations ($[A]^0_{i,j,k}$ and $[G]^0_{i,j,k}$ respectively). As the precursors are oxidised in the chemistry routine which is called before the partitioning is calculated, newly oxidised gas phase products are included with the existing gas phase compounds in $[G]^0$. The final aerosol phase concentration is calculated using:

$$[A]_{i,j,k} = \frac{K_{i,j,k} M_o([A]^0_{i,j,k} + [G]^0_{i,j,k})}{(1 + K_{i,j,k} M_o)} \quad (5)$$

and the final gas phase concentration can be calculated using Eq. (3). The partitioning calculation is performed after every gas phase chemistry integration, in this study every 900 s.

ACPD
7, 9053–9092, 2007

EGU

2.6 SOA and precursor loss processes

A number of loss processes must be included, both for the gas and aerosol phase oxidation products, as well as the precursor hydrocarbons. We assume that 80% of the aerosol phase oxidation products dissolve into cloud droplets when clouds are present and for all the gas phase oxidation products of SOA precursors, a Henry's Law coefficient of $H=1\times10^5\,\mathrm{M\,atm^{-1}}$ is used (Chung and Seinfeld, 2002), with a temperature dependence given by Eq.(6),

$$\frac{dlnH}{dT} = \frac{\Delta H_A}{RT^2} \tag{6}$$

where $\Delta H_A/R=-12\,\mathrm{K}$ (for all precursor hydrocarbons and oxidation products), and ΔH_A is the heat of dissolution. The temperature dependence of the Henry's Law coefficients for the precursor hydrocarbons does not need to be accounted for, and the values used for each class of hydrocarbons are given in Table 7.

Wet deposition related to large scale as well as convective systems is represented in the model, and depends on the amount of precipitation crossing grid box boundaries, which is a model input field. In the case of large scale rain, the cloud fraction and amount of mass exchanged advectively is used to put an upper limit on the amount of a tracer which can be removed from a grid box. An iterative approach is used to calculate condensed water available for taking up gas phase species in convective clouds. The wet deposition routines are described thoroughly in Berglen et al. (2004).

A dry deposition velocity of $0.1\,\mathrm{cm\,s^{-1}}$ is applied in the lowest model layer, for all SOA species (Liousse et al., 1996).

3 Results

In this study, two main model experiments were carried out, in the first ("R_1"), SOA was allowed to condense on existing organic aerosol. In the second experiment ("R_{sulf}"),

SOA was allowed to condense on ammonium sulphate aerosol as well as existing organic aerosol. As a sensitivity test, a third experiment (R_{max}) was run where the mass of the POA was increased so that almost all (more than 99%) of the semi-volatile species formed from the oxidation of SOA precursors partitioned to the aerosol phase. This test then provides the upper limit of the mass of SOA which can be formed in this model, with the current precursor emissions.

3.1 Global Production and Burden of SOA

The total global production of SOA is a very uncertain quantity, as the results of previous modelling studies show. Using a similar approach to that used here, Chung and Seinfeld (2002) estimate a total annual SOA production of about 11.2 Tg yr^{-1}, while Tsigaridis and Kanakidou (2003) suggest that the SOA production from biogenic volatile organic compounds (VOC) might range from 2.5 to 44.5 Tg yr^{-1}, with an additional contribution from anthropogenic VOC of 0.05 to 2.62 Tg yr^{-1}. A range of about 12 Tg yr^{-1} to 70 Tg yr^{-1} of total SOA formation is given by Kanakidou et al. (2005), summarising the results of several different model studies. The total tropospheric SOA production for 2004 was calculated to be 55 Tg yr^{-1}, for R_1, which is within the higher end of the range of these values. The SOA production for 2004 in R_{sulf} was 76 Tg yr^{-1}.

The annual mean SOA burden for 2004, in R_1, was calculated as 0.52 Tg, which is again significantly larger than the 0.19 Tg calculated by Chung and Seinfeld (2002), but closer to the 0.39 Tg calculated by Henze and Seinfeld (2006). Other global estimates of SOA burdens, with SOA schemes of varying complexity include 0.36 Tg (Griffin et al., 1999a), 1.2–1.6 Tg (Kanakidou et al., 2000), 1.4 Tg (Derwent et al., 2003) and 0.05–0.39 Tg (Tsigaridis and Kanakidou, 2003). The SOA burden for R_{sulf} was 0.77 Tg.

One of the reasons that R_1 results in a larger value for total SOA production than that of Chung and Seinfeld (2002), despite a similar treatment of SOA formation, is the inclusion of isoprene as a SOA precursor. This leads to the formation of 15 Tg yr^{-1} of SOA from the isoprene oxidation products (and accounts for about 28 % of the annual average global burden). The additional aerosol mass also leads to an enhancement

ACPD
7, 9053–9092, 2007

of the SOA formation from other hydrocarbons. SOA formation via isoprene oxidation was added to an existing SOA scheme similar to that of Chung and Seinfeld (2002), by Henze and Seinfeld (2006), who found that the global SOA produced directly from the oxidation products of isoprene was 6.2 Tg yr^{-1}, or about 71 % of the production due to other VOC in their model. They also noted that the extra aerosol enhanced the production of SOA from other VOC in their model by 17 %. However, isoprene emissions of around 500 Tg yr^{-1} are used in the model of Henze and Seinfeld (2006) (compared with the 220 Tg yr^{-1} used here), so this can not be the sole explanation for the greater SOA production calculated in the present study.

Other factors which may contribute to the higher SOA burden in our model, as compared to that of Chung and Seinfeld (2002), include the aging rate of the POA, transport of aerosol components by the model and the concentrations (and transport) of oxidants (O_3, OH, NO_3) used. An exponential decay lifetime of 1.15 days was used by Chung and Seinfeld (2002) to convert hydrophobic POA into hydrophilic POA, which is shorter than the 21% day^{-1} used here. Because the formation of SOA depends upon the existing aerosol burden (new particle nucleation was not accounted for), less POA leads to less SOA. With regard to transport, the GISS CTM, which was used by Chung and Seinfeld (2002), has a more rapid transport of tracers from the source regions than the Oslo CTM2 (Schulz et al., 2006). This can reduce POA over areas with high levels of SOA precursors, or it could result in a faster transport of SOA into model levels with clouds, where wet removal is efficient. In addition, differences in cloud water fluxes and precipitation cause different removal rates for a species in two different models, even if the solubility of the species is the same in both models.

As well as the additional SOA source from the inclusion of isoprene in this study, the oxidation products of anthropogenic VOC contribute a further 2.5 Tg yr^{-1} to the annual SOA production in R_1. The contribution of each of the modelled SOA species to the total global SOA production is shown in Table 8. The oxidation products of the class I hydrocarbons make the largest contribution of any species to the global SOA production in both experiments (about 32% in R_1 and 31% in R_{sulf}), mainly due to NO_3

oxidation. The second largest contribution is from the oxidation products of isoprene (27% and 24% in R_1 and R_{sulf} respectively). Allowing the condensation of semi-volatile species on ammonium sulphate aerosols not only increased the total SOA production, but it increased the importance of anthropogenic SOA precursors from about 4.5% in R_1 to almost 9% in R_{sulf}.

The surface concentration and total column amount of SOA for both model runs are shown in Fig. 1, as an annual mean. The regions with the highest SOA concentrations are those where emissions of precursors are highest, for example South America, and Africa. The supply of oxidants and POA has an impact on the SOA concentrations, which are also high in relatively polluted regions such the east coast of North America, parts of Asia, and Europe, where the concentration of POA is highest (Panels D and H). Including the condensation of SOA on ammonium sulphate aerosol generally increases the SOA burden over industrialised areas, especially South East Asia and the east coast of North America, although a smaller increase is also visible over southern Europe (Panels C and G). In R_{sulf}, SOA makes up the majority of the organic aerosol at the surface, on the east coast of North America, however this is not the case in other industrised areas. For the column values, SOA is found to be the dominant contributor to total organic aerosol over part of Europe, as well as a significant part of North America. The major fraction of organic aerosol over Asia, however, remains POA.

3.2 SOA Lifetimes and the contribution of different species to SOA production

The annual average lifetime of SOA was calculated to be 3.2 days in R_1, increasing to 3.7 days in R_{sulf}. Both these values are significantly shorter than the 6.2 days given by Chung and Seinfeld (2002). As the major loss process for SOA in both studies was calculated to be wet deposition (here it was found to be, on average, 95% of the total loss for 2004) and the same scavenging efficiency was used for SOA, the difference probably lies in the calculation of convection and precipitation in the models. The annual mean lifetimes of different species range between about 2.7 and 4.6 days (Table 8), with one of the oxidation products of isoprene having the longest lifetime in

both model runs.

3.3 Comparison with measurements

In order to compare the mass of organic aerosol (OA) that the model predicts with measurements from a number of sites, mean burdens of organic aerosol have been calculated, from both model and measurement data. These values are shown in Table 9. Total OA mass concentration, as well as the concentration of SOA alone are shown for runs R_1 and R_{sulf}, additionally the total OA concentration when all semi-volatile species are partitioned to the aerosol phase is shown (R_{max}).

The measurement data in the first section of Table 9 comes from the Interagency Monitoring of Protected Visual Environments (IMPROVE) Aerosol Network data base, and is a mean of all values available at each selected station for 2004. The stations were selected based on their location, to provide data points spread over most of North America. The modelled values were interpolated to the latitude and longitude of the station and a mean was calculated over the same days as for the measurements. The modelled total organic aerosol values from R_1 are lower than the measured values, for all IMPROVE stations other than Brigantine. However, all modelled values except that for Mammoth Cave NP and Chassahowitzka NWR are within a standard deviation of the mean measured value (although this is partly due to the large variability in the measurements, for example at Denali NP). Values from R_{sulf} are generally closer to the measured values, however there is still a significant underestimation of the measurements. In the model run where SOA partitioned entirely to the aerosol phase, most of the modelled values are close to the observed values, and in several cases, the modelled values are significantly higher than those observed.

For Europe, the model is compared with measurements made during a one year measurement campaign, which took place in 2002 and focused on elemental and organic carbon, as part of the European monitoring and Evaluation programme (EMEP) (Yttri et al., 2007). The modelled data was averaged over the whole year and interpolated to the location of the measurement station. Again, values from R_1 significantly

ACPD
7, 9053–9092, 2007

underestimate the measured values, by around 80%–95% in most cases. Some improvement is seen when the SOA is allowed to partition to the ammonium sulphate aerosol, however, the modelled values remain low. In contrast to what was seen in the comparison with the IMPROVE stations, the results of model run R_{max} are still significantly lower than most of the corresponding observations.

In the third section of Table 9, the modelled data is compared with measurements from stations in countries other than Europe and the USA. Where these measurements were made for less than a whole year, the modelled data is an average of the corresponding time period. The R_1 values are far lower than those measured, and again the R_{sulf} values are generally higher than those in R_1 (except at Aboa). Also for these stations, partitioning all semi-volatile species to the aerosol phase does not produce enough OA to match the observed values.

The fraction of OA which consists of SOA is rather variable and ranges from 0%, at Aboa, to 78% at Mammoth Cave, in run R_{sulf}. At most of the stations, SOA makes up around 30% to 40% of the total modelled OA. Because of the greater existing aerosol mass in R_{sulf}, a higher fraction of OA consists of SOA than is the case in R_1, where typical SOA fractions range between about 10% and 30%, at most stations.

In the last two sections of Table 9, some of the underestimation of the measured OC mass may be explained by the measurements being from a different year than the modelled values. As there are few reported OC measurements for 2004, in most regions it was necessary to use available measurements from other years to compare with the modelled data. Thus an additional uncertainty is introduced in the modelled values, firstly as meteorological conditions may vary between the measurement and modelled periods, bringing different levels of OC from source regions, and secondly as the biomass burning activity varies between years.

Model resolution may also explain a part of the general underestimation of the measured OC values. As the model grid boxes cover relatively large areas, it is not possible for the model to reproduce high OC values associated with either localised emissions, plumes, or topographical features in which aerosol tends to collect, such as large bowls

and valleys.

Although there are a few stations in Table 9 where the SOA values in R_{max} are significantly higher than the observed values, for most locations, even with all semi-volatile organic species partitioned to the aerosol phase (itself an unrealistic scenario), the model underestimates the observed levels of OA. This indicates that the cause of the underestimation does not lie with the partitioning of SOA between gas and aerosol phase, rather that emissions of precursors or POA may be too low. As already noted, the way in which wet deposition is parameterised in the model also plays a role in determining the production and burden of SOA, however comparisons between modelled and measured sulphate aerosol values (not shown), give us confidence that this process is well represented in the Oslo CTM2.

4 Influence of NO_3 on SOA formation

As mentioned above, in this study, the oxidation of SOA precursors by NO_3 is found to lead to a large fraction of the total SOA formation. This is examined in more detail here. As the best match between modelled and observed OA was achieved with R_{sulf}, the analysis below will be restricted to this run.

4.1 Comparison of modelled NO_3 with measurements

The modelled night-time NO_3 concentrations can be compared with measurements from several different locations. Measurements made using a zenith sky spectrometer, were analysed by Allan et al. (2002) to calculate tropospheric profiles of NO_3 during sunrise. Model night-time NO_3 values were calculated for the same locations, during the same months (although the modelled values are from 2004, and the measurements in Allan et al. (2002) were carried out in 1997,1999, and 2000 for Tenerife, Cape Grim and Norway respectively), and are compared with the measured values in Fig. 2. In all three panels of Fig. 2, the modelled values underestimate the measured values,

ACPD
7, 9053–9092, 2007

however there is some overlap of the values within one standard deviation of modelled and measured means, especially in the case of Tenerife and Cape Grim, for the lower altitudes. Further, the model shows the increase in variability in values seen between the surface and about 2 km altitude at Cape Grim, as well as the pronounced gradient in NO_3 concentration at Tenerife.

Night-time modelled NO_3 mixing ratios were calculated and averaged for each month, for the model grid point near Finokalia, Crete, Greece. The results are compared with measurements made in the same area between June 2001 and September 2003 reported by Vrekoussis et al. (2006), in Fig. 3. The model overestimates NO_3 for all months, and most of the measurements are at the lower end of the range of one standard deviation of the model results, except May, where modelled and measured values are similar. The modelled values are elevated between about May and September, the same period for which an increase in the measured NO_3 mixing ratio is seen. The reason for the overestimation is probably related to the model resolution, as emissions from mainland Greece, Lybia and Turkey, as well as Crete itself are included in the model grid boxes surrounding the measurement point. Only emissions originating north of Crete are expected to affect the measurements (Vrekoussis et al., 2006), and these would be more diluted in reality than they are in the model, by the time they reach Crete.

The formation and loss of NO_3 is closely linked with the chemistry of NO and NO_2, therefore a further method of estimating a models representation of NO_3 is to compare the modelled abundance of these species with measurements. Model mixing ratios of NO and NO_2 from Oslo CTM2 have been compared with measurements from Hohenpeissenberg in Germany, in Isaksen et al. (2005), where both the absolute values and the seasonal cycle have been shown to be well reproduced by the model. Tropospheric NO_2 from a range of models is compared with measured values, retrieved from GOME data, by van Noije et al. (2006). The Oslo CTM2 is shown to have one of the higher NO_2 values of the models, and to compare well with measured values.

4.2 SOA production from NO_3 Oxidised Hydrocarbons

The fraction of annual mean SOA produced from precursors which were oxidised by NO_3 is shown in Fig. 4, for the surface (Panel A) and for the total SOA column (Panel B). The effect of NO_3 is much more evident at the surface, and near polluted regions, where emissions of nitrogen oxides coincide with high concentrations of terpenes. In some parts of Asia, up to 60% of the SOA at the surface consists of NO_3 oxidation products. Similarly, high values are seen on the east coast of North America, as well as in Southern Europe. The extremely low contribution of NO_3 oxidation products around Papua New Guinea and parts of Indonesia are due to the formation of a large amount of SOA from isoprene oxidation products as, in the case of isoprene, only oxidation by OH can lead to SOA in this model. The influence of NO_3 on the total SOA column, shown in panel B of Fig. 4, is much more uniform, with values over land in the northern hemisphere being between 30% and 45%. Again, the fraction is highest over India and south eastern China, and the east coast of North America.

5 Summary and conclusions

A new module has been added to the Oslo CTM2, allowing the simulation of SOA formation, transport and loss. The calculated annual production (55–76 Tg yr^{-1}) and burden (0.43–0.77 Tg) of SOA are at the high end of the range of the results of previous model studies. The amount of SOA was increased by allowing semi-volatile species to partition to ammonium sulphate aerosol as well as organic aerosol, and this lead to modelled OA values which were closer to the observed values than when only partitioning to pre-existing organic aerosol was allowed. Despite this improvement, the model still underestimates OA at most of the observation stations. Modelled OA values remain too low, especially in Europe, even when all semi-volatile species are partitioned to the aerosol phase, which suggests that the reason for the model underestimation of OA lies with the source of either POA or precursors of SOA. Increasing

ACPD
7, 9053–9092, 2007

EGU

the isoprene emissions in the model to bring them more in line with recent estimates will increase the SOA production, however, this is unlikely to substantially reduce the underestimation of OA over Europe.

Further reduction of the uncertainties in emission estimates for POA, and SOA precursors would help reduce the uncertainties in modelling SOA formation. It is also apparent that similar SOA schemes can produce rather different results when combined with different global CTMs, possibly due to differences in the calculation of wet deposition of SOA components as well as differences in advective and convective transport.

The results of this study show a significantly higher contribution of NO_3 oxidation products to the SOA burden than that found in previous studies. Regionally this contribution reached up to 60%, and the global annual mean contribution was found to be about 29 %.

The contrast in the contribution of NO_3 oxidation products to the SOA burden between regions with high anthropogenic emissions and relatively unpolluted regions also highlights the importance of the anthropogenic influence on the oxidising capacity of the atmosphere, for regional SOA formation.

Many global models still treat SOA in a similar fashion to POA, i.e. as a direct emission, or do not include SOA at all (Textor et al., 2006). Representing SOA as a direct emission is too simplistic since the concentration of SOA has been shown, in both this and previous works, to depend upon a wide range of factors, such as emissions of precursors, oxidation compounds, and the loading of aerosols upon which SOA may condense. In industrialised and biomass burning regions SOA accounts for an important fraction of the total OA. In biomass burning regions global models tend to underestimate the observed total aerosol optical depth (AOD) (Myhre et al., 2003; Kinne et al., 2006). Given the significant contribution of SOA to the total OA burden, a more realistic representation, in global aerosol models, of processes governing the SOA burden will reduce model underestimates of the AOD.

Acknowledgements. This work was supported by funding from BACCI (research unit on Biosphere-Aerosol-Cloud-Climate-Interactions), as well as AerOzClim (Aerosols, Ozone and

Climate, NFR project number 142050).

References

Ackerman, A. S., Toon, O. B., Stevens, D. E., Heymsfield, A. J., Ramanathan, V., and Welton, E. J.: Reduction of Tropical Cloudiness by Soot, Science, 288, 1042–1047, 2000. 9055

Albrecht, B. A.: Aerosols, Cloud Microphysics, and Fractional Cloudiness, Science, 245, 1227–1230, 1989. 9055

Allan, B. J., Plane, J. M. C., Coe, H., and Shillito, J.: Observations of NO_3 concentration profiles in the troposphere, J. Geophys. Res., 107, 4588, doi:10.1029/2002JD002112, 2002. 9056, 9068, 9090

Berglen, T. F., Berntsen, T. K., Isaksen, I. S. A., and Sundet, J. K.: A global model of the coupled sulfur/oxidant chemistry in the troposphere: The sulfur cycle, J. Geophys. Res., 109, D19310, doi:10.1029/2003JD003948, 2004. 9057, 9062

Berntsen, T. K. and Isaksen, I. S. A.: A global three-dimensional chemical transport model for the troposphere 1. Model description and CO and ozone results, J. Geophys. Res., 102, 21 239–21 280, doi:10.1029/97JD01140, 1997. 9057

Bond, T. C., Streets, D. G., Yarber, K. F., Nelson, S. M., Woo, J.-H., and Klimont, Z.: A technology-based global inventory of black and organic carbon emissions from combustion, J. Geophys. Res.-Atmos., 109, D14203, doi:10.1029/2003JD003697, 2004. 9060, 9081

Brown, S. S., Osthoff, H. D., Stark, H., Dubé, W. P., Ryerson, T. B., Warneke, C., de Gouw, J. A., Wollny, A. G., Parrish, D. D., Fehsenfeld, F. C., and Ravishankara, A. R.: Aircraft observations of daytime NO_3 and N_2O_5 and their implications for tropospheric chemistry, J. Photoch. Photobio. A, 176, 270–278, 2005. 9056

Brunner, D., Staehelin, J., Rogers, H. L., Köhler, M. O., Pyle, J. A., Hauglustaine, D., Jourdain, L., Berntsen, T. K., Gauss, M., Isaksen, I. S. A., Meijer, E., van Velthoven, P., Pitari, G., Mancini, E., Grew, V., and Sausen, R.: An evaluation of the performance of chemistry transport models by comparison with research aircraft observations. Part 1: Concepts and overall model performance, Atmos. Chem. Phys., 3, 1609–1631, 2003, http://www.atmos-chem-phys.net/3/1609/2003/. 9057

Chung, S. H. and Seinfeld, J. H.: Global distribution and climate forcing of carbonaceous

aerosols, J. Geophys. Res.-Atmos., 107, 4407, doi:10.1029/2001JD001397, 2002. 9055, 9056, 9058, 9060, 9061, 9062, 9063, 9064, 9065, 9082

Cooke, W. F., Liousse, C., Cachier, H., and Feichter, J.: Construction of a 1°x1° fossil fuel emission data set for carbonaceous aerosol and implementation and radiative impact in the ECHAM4 model, J. Geophys. Res., 104, 22 137–22 162, doi:10.1029/1999JD900187, 1999. 9055, 9059

Derwent, R. G., Collins, W. J., Jenkin, M. E., Johnson, C. E., and Stevenson, D. S.: The Global Distribution of Secondary Particulate Matter in a 3-D Lagrangian Chemistry Transport Model, J. Atmos. Chem., 44, 57–95, 2003. 9056, 9063

Dindorf, T., Kuhn, U., Ganzeveld, L., Schebeske, G., Ciccioli, P., Holzke, C., Köble, R., Seufert, G., and Kesselmeier, J.: Significant light and temperature dependent monoterpene emissions from European beech (Fagus sylvatica L.) and their potential impact on the European volatile organic compound budget, J. Geophys. Res.-Atmos., 111, D16305, doi:10.1029/2005JD006751, 2006. 9058

Granier, C., Lamarque, J. F., Mieville, A., Muller, J. F., Olivier, J., Orlando, J., Peters, J., Petron, G., Tyndall, G., and Wallens, S.: POET, a database of surface emissions of ozone precursors, available on internet at http://www.aero.jussieu.fr/projet/ACCENT/POET.php, 2005. 9057, 9058, 9081

Griffin, R. J., Cocker, D. R., Seinfeld, J. H., and Dabdub, D.: Estimate of global atmospheric organic aerosol from oxidation of biogenic hydrocarbons, Geophys. Res. Lett., 26, 2721–2724, doi:10.1029/1999GL900476, 1999a. 9056, 9058, 9063

Griffin, R. J., Flagan, R. C., and Seinfeld, J. H.: Organic aerosol formation from the oxidation of biogenic hydrocarbons, J. Geophys. Res., 104, 3555–3568, doi:10.1029/1998JD100049, 1999b. 9060

Guenther, A., Hewitt, C. N., Erickson, D., Fall, R., Geron, C., Graedel, T., Harley, P., Klinger, L., Lerdau, M., McKay, W. A., Pierce, T., Scholes, B., Steinbrecher, R., Tallamraju, R., Taylor, J., and Zimmerman, P.: A global model of natural volatile organic compound emissions, J. Geophys. Res., 100, 8873–8892, doi:10.1029/94JD02950, 1995. 9057, 9058, 9059, 9081

Guenther, A., Karl, T., Harley, P., Wiedinmyer, C., Palmer, P. I., and Geron, C.: Estimates of global terrestrial isoprene emissions using MEGAN (Model of Emissions of Gases and Aerosols from Nature), Atmos. Chem. Phys., 6, 3181–3210, 2006, http://www.atmos-chem-phys.net/6/3181/2006/. 9058

Han, J. S., Moon, K. J., Kong, B. J., Lee, S. J., Kim, J. E., and Kim, Y. J.: Seasonal variation

of chemical composition in fine particles at Gosan, Korea, Environ. Monit. Assess., 107, 221–237, 2005. 9088
Hansen, J., Sato, M., and Ruedy, R.: Radiative forcing and climate response, J. Geophys. Res., 102, 6831–6864, doi:10.1029/96JD03436, 1997. 9055
Haywood, J. M. and Shine, K. P.: The effect of anthropogenic sulfate and soot aerosol on the clear sky planetary radiation budget, Geophys. Res. Lett., 22, 603–606, doi:10.1029/95GL00075, 1995. 9055
Henze, D. K. and Seinfeld, J. H.: Global secondary organic aerosol from isoprene oxidation, Geophys. Res. Lett., 33, doi:10.1029/2006GL025976, 2006. 9056, 9061, 9063, 9064, 9083
Hesstvedt, E., Hov, Ø., and Isaksen, I. S. A.: Quasi-Steady-State Approximations in Air-Pollution Modeling - Comparison of Two Numerical Schemes for Oxidant Prediction, Int. J. Chem. Kinet., 10, 971–994, 1977. 9057
Hoffmann, T., Odum, J. R., Bowman, F., D.Collins, Klockow, D., Flagan, R. C., and Seinfeld, J. H.: Formation of Organic Aerosols from the Oxidation of Biogenic Hydrocarbons, J. Atmos. Chem., 26, 189–222, 1997. 9060
Holtslag, A. A. M. and Ulden, A. P. V.: A Simple Scheme for Daytime Estimates of the Surface Fluxes from Routine Weather Data, J. Clim. Appl. Meteorol., 22, 517–529, 1983. 9059
IPCC: Climate Change 2001: The Scientific Basis. Contribution of Working Group I to the Third Assessment Report of the Intergovernmental Panel on Climate Change, Cambridge University Press, Cambridge, United Kingdom and New York, NY, USA, 881pp., 2001. 9058, 9081
Isaksen, I. S. A., Zerefos, C., Kourtidis, K., Meleti, C., Dalsoren, S. B., Sundet, J. K., Grini, A., Zanis, P., and Balis, D.: Tropospheric ozone changes at unpolluted and semipolluted regions induced by stratospheric ozone changes, J. Geophys. Res., 110, D02302, doi:10.1029/2004JD004618, 2005. 9057, 9069
Jones, A. P.: Indoor air quality and health, Atmos. Environ., 33, 4535–4564, 1999. 9055
Kanakidou, M., Tsigaridis, K., Dentener, F. J., and Crutzen, P. J.: Human-activity-enhanced formation of organic aerosols by biogenic hydrocarbon oxidation, J. Geophys. Res., 105, 9243–9254, doi:10.1029/1999JD901148, 2000. 9056, 9063
Kanakidou, M., Seinfeld, J. H., Pandis, S. N., Barnes, I., Dentener, F. J., Facchini, M. C., van Dingenen, R., Ervens, B., Nenes, A., Nielsen, C. J., Swietlicki, E., Putaud, J. P., Balkanski, Y., Fuzzi, S., Horth, J., Moortgat, G. K., Winterhalter, R., Myhre, C. E. L., Tsigaridis, K., Vignati, E., Stephanou, E. G., and Wilson, J.: Organic aerosol and global climate modelling:

a review, Atmos. Chem. Phys., 5, 1053–1123, 2005, http://www.atmos-chem-phys.net/5/1053/2005/. 9055, 9058, 9059, 9063

Kesselmeier, J. and Staudt, M.: Biogenic Volatile Organic Compounds (VOC): An Overview on Emission, Physiology and Ecology, J. Atmos. Chem., 33, 23–88, 1999. 9058

Kinne, S., Schulz, M., Textor, C., Guibert, S., Balkanski, Y., Bauer, S. E., Berntsen, T., Berglen, T. F., Boucher, O., Chin, M., Collins, W., Dentener, F., Diehl, T., Easter, R., Feichter, J., Fillmore, D., Ghan, S., Ginoux, P., Gong, S., Grini, A., Hendricks, J., Herzog, M., Horowitz, L., Isaksen, I., Iversen, T., Kirkevåg, A., Kloster, S., Koch, D., Kristjansson, J. E., Krol, M., Lauer, A., Lamarque, J. F., Lesins, G., Liu, X., Lohmann, U., Montanaro, V., Myhre, G., Penner, J., Pitari, G., Reddy, S., Seland, O., Stier, P., Takemura, T., and Tie, X.: An AeroCom initial assessment - optical properties in aerosol component modules of global models, Atmos. Chem. Phys., 6, 1815–1834, 2006, http://www.atmos-chem-phys.net/6/1815/2006/. 9071

Kuhn, U., Rottenberger, S., Biesenthal, T., Wolf, A., Schebeske, G., Ciccioli, P., Brancaleoni, E., Frattoni, M., Tavares, T. M., and Kesselmeier, J.: Isoprene and monoterpene emissions of Amazônian tree species during the wet season: Direct and indirect investigations on controlling environmental functions, J. Geophys. Res.-Atmos., 107, 8069, doi:10.1029/2000JD000303, 2002. 9058

Lathière, J., Hauglustaine, D. A., Friend, A. D., de Noblet-Ducoudré, N., Viovy, N., and Folberth, G. A.: Impact of climate variability and land use changes on global biogenic volatile organic compound emissions, Atmos. Chem. Phys., 6, 2129–2146, 2006, http://www.atmos-chem-phys.net/6/2129/2006/. 9058

Liousse, C., Penner, J. E., Chuang, C., Walton, J. J., Eddleman, H., and Cachier, H.: A global three-dimensional model study of carbonaceous aerosols, J. Geophys. Res., 101, 19 411–19 432, doi:10.1029/95JD03426, 1996. 9055, 9062

Maria, S. F., Russell, L. M., Gilles, M. K., and Myneni, S. C. B.: Organic Aerosol Growth Mechanisms and Their Climate-Forcing Implications, Science, 306, 1921–1924, doi:10.1126/science.1103491, 2004. 9060

S.Moukhtar, S., Bessagnet, B., Rouil, L., and Simon, V.: Monoterpene emissions from Beech (Fagus sylvatica) in a French forest and impact on secondary pollutants formation at regional scale, Atmos. Environ., 39, 3535–3547, 2005. 9058

Myhre, G., Berntsen, T. K., Haywood, J. M., Sundet, J. K., Holben, B. N., Johnsrud, M., and Stordal, F.: Modelling the solar radiative impact of aerosols from biomass burning during

the Southern African Regional Science Initiative (SAFARI-2000) experiment, J. Geophys. Res.-Atmos., 108, 37–1, doi:10.1029/2002JD002313, 2003. 9071

Myhre, G., Bellouin, N., Berglen, T. F., Berntsen, T. K., Boucher, O., Grini, A., Isaksen, I. S. A., Johnsrud, M., Mishchenko, M. I., Stordal, F., and Tanré, D.: Comparison of the radiative properties and direct radiative effect of aerosols from a global aerosol model and remote sensing data over ocean, Tellus B, 59, 115–129, doi:10.1111/j.1600-0889.2006.00226.x, 2007. 9057

Ostro, B. and Chestnut, L.: Assessing the health benifits of reducing particulate matter air pollution in the United States, Environ. Res., 76, 94–106, 1998. 9055

Penkett, S. A., Blake, N. J., Lightman, P., Marsh, A. R. W., Anwyl, P., and Butcher, G.: The seasonal variation of nonmethane hydrocarbons in the free troposphere over the North Atlantic Ocean - Possible evidence for extensive reaction of hydrocarbons with the nitrate radical, J. Geophys. Res., 98, 2865–2885, 1993. 9056

Penner, J. E., Chuang, C. C., and Grant, K.: Climate forcing by carbonaceous and sulfate aerosols, Clim. Dynam., 14, 839–851, 1998. 9055

Pun, B. K., Wu, S.-Y., Seigneur, C., Seinfeld, J. H., Griffin, R. J., and Pandis, S. N.: Uncertainties in Modeling Secondary Organic Aerosols: Three-Dimensional Modeling Studies in Nashville/Western Tennessee, Environ. Sci. Technol., 37, 3647–3661, 2003. 9055

Puxbaum, H., Rendl, J., Allabashi, R., Otter, L., and Scholes, M. C.: Mass balance of the atmospheric aerosol in a South African subtropical savanna (Nylsvley, May 1997), J. Geophys. Res., 105, 20 697–20 706, doi:10.1029/2000JD900306, 2000. 9088

Robinson, A. L., Donahue, N. M., Shrivastava, M. K., Weitkamp, E. A., Sage, A. M., Grieshop, A. P., Lane, T. E., Pierce, J. R., and Pandis, S. N.: Rethinking Organic Aerosols: Semivolatile Emissions and Photochemical Aging, Science, 315, 1262, doi:10.1126/science.1133061, 2007. 9055

Schulz, M., Textor, C., Kinne, S., Balkanski, Y., Bauer, S., Berntsen, T., Berglen, T., Boucher, O., Dentener, F., Guibert, S., Isaksen, I. S. A., Iversen, T., Koch, D., Kirkevåg, A., Liu, X., Montanaro, V., Myhre, G., Penner, J. E., Pitari, G., Reddy, S., Seland, Ø., Stier, P., and Takemura, T.: Radiative forcing by aerosols as derived from the AeroCom present-day and pre-industrial simulations, Atmos. Chem. Phys., 6, 5225–5246, 2006, http://www.atmos-chem-phys.net/6/5225/2006/. 9055, 9057, 9064

Smith, D. J. T., Harrison, R. M., Luhana, L., Pio, C. A., Castro, L. M., Tariq, M. N., Hayat, S., and Quraishi, T.: Global modelling of secondary organic aerosol in the troposphere: A sensitivity

analysis, Atmos. Environ., 30, 4031–4040, 1996. 9088
Takami, A., Miyoshi, T., Shimono, A., and Hatakeyama, S.: Chemical composition of fine aerosol measured by AMS at Fukue Island, Japan during APEX period, Atmos. Environ., 39, 4913–4924, 1995. 9088
Textor, C., Schulz, M., Guibert, S., Kinne, S., Balkanski, Y., Bauer, S., Berntsen, T., Berglen, T., Boucher, O., Chin, M., Dentener, F., Diehl, T., Easter, R., Feichter, H., Fillmore, D., Ghan, S., Ginoux, P., Gong, S., Grini, A., Hendricks, J., Horowitz, L., Huang, P., Isaksen, I., Iversen, I., Kloster, S., Koch, D., Kirkevåg, A., Kristjansson, J. E., Krol, M., Lauer, A., Lamarque, J. F., Liu, X., Montanaro, V., Myhre, G., Penner, J., Pitari, G., Reddy, S., Seland, Ø., Stier, P., Takemura, T., and Tie, X.: Analysis and quantification of the diversities of aerosol life cycles within AeroCom, Atmos. Chem. Phys., 6, 1777–1813, 2006, http://www.atmos-chem-phys.net/6/1777/2006/. 9071
Tsigaridis, K. and Kanakidou, M.: Global modelling of secondary organic aerosol in the troposphere: A sensitivity analysis, Atmos. Chem. Phys., 3, 2879–2929, 2003, http://www.atmos-chem-phys.net/3/2879/2003/. 9055, 9056, 9063
Tsigaridis, K., Lathière, J., Kanakidou, M., and Hauglustaine, D. A.: Naturally driven variability in the global secondary organic aerosol over a decade, Atmos. Chem. Phys., 5, 1891–1904, 2005, http://www.atmos-chem-phys.net/5/1891/2005/. 9056
Twomey, S.: The Nuclei of Natural Cloud Formation Part II: The Supersaturation in Natural Clouds and the Variation of Cloud Droplet Concentration, Geofisica pura e applicata, 43, 243–249, 1959. 9055
Twomey, S.: The Influence of Pollution on the Shortwave Albedo of Clouds, J. Atmos. Sci., 34, 1149–1152, 1977. 9055
van der Werf, G. R., Randerson, J. T., Giglio, L., Collatz, G. J., Kasibhatla, P. S., and Arellano, Jr., A. F.: Interannual variability in global biomass burning emissions from 1997 to 2004, Atmos. Chem. Phys., 6, 3423–3441, 2006, http://www.atmos-chem-phys.net/6/3423/2006/. 9060, 9081
van Noije, T. P. C., Eskes, H. J., Dentener, F. J., Stevenson, D. S., Ellingsen, K., Schultz, M. G., Wild, O., Amann, M., Atherton, C. S., Bergmann, D. J., Bey, I., Boersma, K. F., Butler, T., Cofala, J., Drevet, J., Fiore, A. M., Gauss, M., Hauglustaine, D. A., Horowitz, L. W., Isaksen, I. S. A., Krol, M. C., Lamarque, J.-F., Lawrence, M. G., Martin, R. V., Montanaro, V., Müller, J.-F., Pitari, G., Prather, M. J., Pyle, J. A., Richter, A., Rodriguez, J. M., Savage, N. H., Strahan,

S. E., Sudo, K., Szopa, S., and van Roozendael, M.: Multi-model ensemble simulations of tropospheric NO_2 compared with GOME retrievals for the year 2000, Atmos. Chem. Phys., 6, 2943–2979, 2006, http://www.atmos-chem-phys.net/6/2943/2006/. 9069

Virkkula, A., Teinilã, K., Hillamo, R., V.-M.Kerminen, Saarikoski, S., Aurela, M., J.Viidanoja, Paatero, J., Koponen, I. K., and Kulmala, M.: Chemical composition of boundary layer aerosol over the Atlantic Ocean and at an Antarctic site, Atmos. Chem. Phys., 6, 3407–3421, 2006, http://www.atmos-chem-phys.net/6/3407/2006/. 9088

Volkamer, R., Jimenez, J. L., San Martini, F., Dzepina, K., Zhang, Q., Salcedo, D., Molina, L. T., Worsnop, D. R., and Molina, M. J.: Secondary organic aerosol formation from anthropogenic air pollution: Rapid and higher than expected, Geophys. Res. Lett., 33, L17811, doi:10.1029/2006GL026899, 2006. 9055

Vrekoussis, M., Kanakidou, M., Mihalopoulos, N., Crutzen, P. J., Lelieveld, J., Perner, D., Berresheim, H., and Baboukas, E.: Role of the NO_3 radicals in oxidation processes in the eastern Mediterranean troposphere during the MINOS campaign, Atmos. Chem. Phys., 4, 169–182, 2004, http://www.atmos-chem-phys.net/4/169/2004/. 9056

Vrekoussis, M., Liakakou, E., Mihalopoulos, N., Kanakidou, M., Crutzen, P. J., and Lelieveld, J.: Formation of HNO_3 and NO_3^- in the anthropogenically-influenced eastern Mediterranean marine boundary layer, Geophys. Res. Lett., 33, L05811, doi:10.1029/2005GL025069, 2006. 9069, 9091

Yang, H., Yu, J. Z., Ho, S. S. H., Xu, J., W.-S.Wu, Wan, C. H., Wang, X., Wang, X., and Wang, L.: The chemical composition of inorganic and carbonaceous materials in $PM_{2.5}$ in Nanjing, China, Atmos. Environ., 39, 3735–3749, 2005. 9088

Yttri, K. E., Aas, W., Bjerke, A., Ceburnis, D., Dye, C., Emblico, L., Facchini, M. C., Forster, C., Hanssen, J. E., Hansson, H. C., Jennings, S. G., Maenhaut, W., Putaud, J. P., , and Trseth, K.: Elemental and organic carbon in PM_{10}: a one year measurement campaign within the European Monitoring and Evaluation Programme EMEP, Atmos. Chem. Phys. Discuss., 7, 3859–3899, 2007, http://www.atmos-chem-phys-discuss.net/7/3859/2007/. 9066

Zhang, Q., Worsnop, D. R., Canagaratna, M. R., and Jimenez, J. L.: Hydrocarbon-like and oxygenated organic aerosols in Pittsburgh: insights into sources and processes of organic

aerosols, Atmos. Chem. Phys., 5, 3289–3311, 2005,
http://www.atmos-chem-phys.net/5/3289/2005/. 9055

Table 1. The class to which the different precursors are assigned, and the fraction of the biogenic emissions they account for.

Monoterpenes	Contribution (%) and class	
α-Pinene	35,	I
β-Pinene	23,	I
Limonene	23,	II
Myrcene	5,	IV
Sabinene	5,	I
Δ^3-Carene	4,	I
Ocimene	2,	IV
Terpinolene	2,	III
$\alpha-$ &$\gamma-$Terpinene	1,	III
ORVOC		
Terpinoid Alcohols	9,	IV
Sesquiterpenes	5,	V
Terpenoid Ketones	4,	I

Table 2. Global, annual emissions of organic compounds used in Oslo CTM2 for this study. [1]Other Reactive Volitile Organic Compounds (ORVOC).

Species	Emission	Reference
Toluene	7.1 Tg yr^{-1}	Schultz et al. (2007)[1]
M-xylene	5.5 Tg yr^{-1}	Schultz et al. (2007)[1]
Trimethylbenzene	1.1 Tg yr^{-1}	Schultz et al. (2007)[1]
Other aromatics	3.4 Tg yr^{-1}	Schultz et al. (2007)[1]
Monoterpenes	127 Tg(C) yr^{-1}	Guenther et al. (1995)
ORVOC[1]	259 Tg(C) yr^{-1}	Guenther et al. (1995)
Isoprene	220 Tg yr^{-1}	Granier et al. (2005), IPCC (2001)
POA (bio/fossil fuel)	8.8 Tg(C) yr^{-1}	Bond et al. (2004)
POA (biomass burning)	21.5 Tg yr^{-1}	van der Werf et al. (2006)

Table 3. Reaction rates, taken from Chung and Seinfeld (2002). The temperature dependence of the rate constants is given by $\frac{k(T_2)}{k(T_1)} = \exp[-\frac{E}{R}(\frac{1}{T_2} - \frac{1}{T_1})]$, where T_1 and T_2 are temperatures in K, E is the activation energy and R is the gas constant. The value of E/R for α-Pinene oxidation is used for all classes, i.e. 732 K, –400 K, –490 K for reaction with O_3, OH and NO_3 respectively.

Hydrocarbon	$k_{O_3} \times 10^{18}$	$k_{OH} \times 10^{12}$	$k_{NO_3} \times 10^{12}$
Class I	56	84	7
Class II	200	171	12
Class III	7700	255	89
Class IV	423	199	15
Class V	11,650	245	27

Table 4. Reaction rates used for aromatics and isoprene. The temperature dependence of the reaction rates is given by $k = A * \exp(B/T)$, where T is the temperature in K. Isoprene reaction with OH was considered to be the major pathway leading to SOA formation, reaction with O_3 or NO_3 was ignored (Henze and Seinfeld, 2006). Reactions without a temperature dependence are indicated by N/A. The reaction rates for m-xylene are the average of those for the *ortho-*, *meta-* and *para-* isomers. For reaction with O3, this is[a]: $(2.4\times10^{-13}\exp(-5586/T) + 5.37\times10^{-13}\exp(-6039/T) + 1.91\times10^{-13}\exp(-5586/T))/3$.

	O_3		OH	
	A	*B*	*A*	*B*
Toluene	2.34×10^{-12}	–6694	5.96×10^{-12}	N/A
M-Xylene	*a*	*a*	1.72×10^{-11}	N/A
Isoprene	–	–	2.54×10^{-11}	410.0

Table 5. Mass based stoichiometric coefficients for the products formed by oxidation of the precursor hydrocarbons.[a] The only oxidant considered for isoprene is OH.

Hydrocarbon	$OH + O_3$ oxidation		NO_3 oxidation
	$\alpha_{i,1,1}$	$\alpha_{i,1,2}$	$\alpha_{i,2,1}$
Class I	0.067	0.354	1.0
Class II	0.239	0.363	1.0
Class III	0.069	0.201	1.0
Class IV	0.067	0.135	1.0
Class V	1.0	–	1.0
Toluene	0.071	0.138	–
M-Xylene	0.038	0.167	–
Isoprene[a]	0.232	0.0288	–

Table 6. Gas to aerosol phase partitioning coefficients at 298 K, [a] except for products of isoprene oxidation (specified at 295 K). [b] The only oxidant considered for isoprene is OH.

Hydrocarbon	OH + O_3 oxidation		NO_3 oxidation
	$K_{i,1,1}$	$K_{i,1,2}$	$K_{i,2,1}$
class I	0.184	0.0043	0.0163
class II	0.055	0.0053	0.0163
class III	0.133	0.0035	0.0163
class IV	0.224	0.0082	0.0163
class V	0.0459	–	0.0163
Toluene	0.053	0.0019	–
M-Xylene	0.042	0.0014	–
Isoprene[a,b]	0.00862	1.62	–

Table 7. The Henry's Law coefficients used for the biogenic parent hydrocarbons, the biogenic oxidation products (including isoprene)[a], all of the aromatic oxidation products[b], except product 1 of m-xylene oxidation[c].

Class	H ($M\,atm^{-1}$ at 298 K)
I	0.023
II	0.07
III	0.067
IV	54
V	0.049
Bio. Prod.[a]	1×10^5
Aromat.Prod.[b]	1×10^3
Prod. 1 m-xylene[c]	1×10^4

Table 8. The lifetimes and contribution to total SOA production of the modelled SOA species. Subscript indexes correspond to the *i*'s and *j*'s and *k*'s in Table 5. The first set of numbers are from R_1, whereas those in brackets are from R_{sulf}.

Species	lifetime (hours)	Contribution to production (%)
SOA_{111}	95.4 (101.0)	6.2(5.7)
SOA_{211}	88.0 (95.4)	5.5(5.3)
SOA_{311}	92.6 (98.5)	0.29(0.3)
SOA_{411}	90.0 (94.8)	2.5(2.3)
SOA_{511}	82.3 (89.8)	11.5(11.2)
SOA_{611}	78.5 (86.1)	17.8(16.8)
SOA_{711}	65.8 (77.9)	0.36(0.3)
SOA_{811}	72.4 (90.7)	1.3(1.4)
SOA_{112}	74.2 (80.7)	8.8(8.3)
SOA_{212}	74.5 (81.2)	3.5(3.4)
SOA_{312}	73.7 (79.8)	0.2(0.2)
SOA_{412}	74.7 (81.8)	1.7(1.6)
SOA_{612}	109.7(111.5)	8.9(7.2)
SOA_{712}	68.3 (69.4)	1.2(1.1)
SOA_{812}	67.7 (72.1)	1.7(5.9)
SOA_{121}	72.7 (88.2)	16.7(17.0)
SOA_{221}	72.3 (88.0)	3.3(3.5)
SOA_{321}	73.2 (89.7)	0.3(0.3)
SOA_{421}	72.4 (87.7)	7.3(7.5)
SOA_{521}	73.4 (89.8)	0.7(0.7)

Table 9. A comparison between measured and modelled total organic matter (OM), for the three model experiments, R_1 R_{sulf} and R_{max}. Also shown is the SOA component of the OM for these runs. [1]EMEP measurements are annual means for 2002.[2] Puxbaum et al. (2000),[3] Smith et al. (1996),[4] Han et al. (2005),[5]Takami et al. (1995),[6] Yang et al. (2005), [7] Virkkula et al. (2006).

Station	lat (degN)	lon (degE)	alt (m)	meas. OM ($\mu g\,m^{-3}$)	OM (R_1) ($\mu g\,m^{-3}$)	SOA (R_1) ($\mu g\,m^{-3}$)	OM (R_{sulf}) ($\mu g\,m^{-3}$)	SOA (R_{sulf}) ($\mu g\,m^{-3}$)	OM (R_{max}) ($\mu g\,m^{-3}$)
Brigantine NWR	39.47	–74.45	5	2.19±1.34	3.18±2.29	0.98±1.42	3.98 ±3.17	1.79 ±2.41	7.10±6.60
Chassahowitzka NWR	28.75	–82.55	4	2.65±1.49	1.11±0.77	0.48±0.60	1.95 ±1.59	1.32 ±1.48	7.24±5.31
Denali NP	63.72	–148.97	658	5.25±17.34	1.06±2.35	0.12±0.25	1.06 ±2.33	0.12 ±0.23	1.28±2.54
Hawaii Volcanoes NP	19.43	–155.26	1258	0.25±0.22	0.06±0.04	0.00±0.01	0.08 ±0.07	0.03 ±0.06	0.24±0.32
Mammoth Cave NP	37.13	–86.15	235	2.56±1.20	1.05±0.76	0.51±0.63	2.50 ±2.38	1.96 ±2.30	7.14±7.09
Mount Rainier NP	46.76	–122.12	439	1.79±1.57	0.54±0.49	0.11±0.17	0.60 ±0.54	0.17 ±0.25	1.87±2.24
Virgin Islands NP	18.34	–64.80	51	0.20±0.25	0.11±0.07	0.02±0.02	0.18 ±0.12	0.09 ±0.07	0.80±0.61
Weminuche Wilderness	37.66	–107.80	2750	0.80±0.69	0.13±0.09	0.04±0.05	0.23 ±0.23	0.14 ±0.20	0.72±0.81
Yellowstone NP 2	44.57	–110.40	2425	0.98±0.88	0.21±0.38	0.07±0.15	0.26 ±0.43	0.12 ±0.21	0.82±1.09
Yosemite NP	37.71	–119.71	1603	2.91±6.73	0.24±0.19	0.05±0.07	0.28 ±0.23	0.09 ±0.13	1.18±1.30
Košetice	49.35	15.05	534	6.41±3.65[1]	0.71 ±0.29	0.11 ±0.11	1.02 ±0.56	0.42 ±0.43	2.03 ±1.59
Virolahti	60.31	27.41	4	3.54±3.16[1]	1.60 ±1.60	0.29 ±0.40	1.91 ±1.74	0.61 ±0.86	3.62 ±3.57
Langenbrügge	52.48	10.45	74	7.31±5.80[1]	0.79±0.45	0.13±0.15	1.06 ±0.69	0.41 ±0.46	2.17±1.93
Kollumerwaard	53.20	6.17	1	4.40±3.25[1]	1.03 ±0.49	0.13 ±0.18	1.25 ±0.74	0.35 ±0.47	2.06 ±1.78
Mace Head	53.20	–9.54	340	1.68±1.81[1]	0.13±0.10	0.02 ±0.02	0.21 ±0.16	0.09 ±0.09	0.37±0.34
Ispra	45.48	8.38	209	12.46±10.88[1]	0.63 ±0.24	0.10 ±0.10	0.91 ±0.47	0.38 ±0.38	2.05 ±1.65
Birkenes	58.23	8.15	190	2.67±2.62[1]	0.35 ±0.32	0.06 ±0.11	0.51 ±0.52	0.22 ±0.32	1.11 ±1.53
Braganca	41.49	–6.46	691	7.38±8.39[1]	0.39±0.29	0.06 ±0.05	0.54 ±0.36	0.21 ±0.16	1.14±0.82
Aspvreten	58.48	17.23	20	3.39±2.72[1]	0.71 ±0.47	0.12 ±0.16	0.90 ±0.66	0.31 ±0.41	1.93 ±1.89
Stará Lesná	49.09	20.17	808	6.48±4.34[1]	0.80 ±0.35	0.14 ±0.15	1.17 ±0.73	0.51 ±0.57	2.07 ±1.70
Nylsvley NR, South Africa[2]	24.39	28.24	1000	22.56	0.21±0.04	0.01±0.00	0.28 ±0.07	0.08±0.04	0.82±0.12
Lahore, Pakistan[3]	31.34	74.22	209	132.64±62.24	2.38±0.77	0.43±0.36	2.83±1.18	0.87 ±0.88	5.78±2.80
Gosan, Korea[4]	33.17	126.1	70	3.44±2.96	1.18±0.65	0.12±0.18	1.54±1.02	0.49±0.72	2.45±1.95
Fukue Island, Japan[5]	32.8	128.7	27	5.03	1.35±0.79	0.06±0.06	1.47±0.89	0.18 ±0.18	1.86±1.17
Nanjing, China[6]	32.04	118.49	267	22.79	3.30±1.65	0.11±0.10	3.45 ±1.79	0.26±0.28	3.77±2.00
Aboa, Antarctica[7]	73.03	-13.05	470	0.12±0.07	0.05±0.05	0.00±0.00	0.05±0.05	0.0±0.0	0.05±0.05

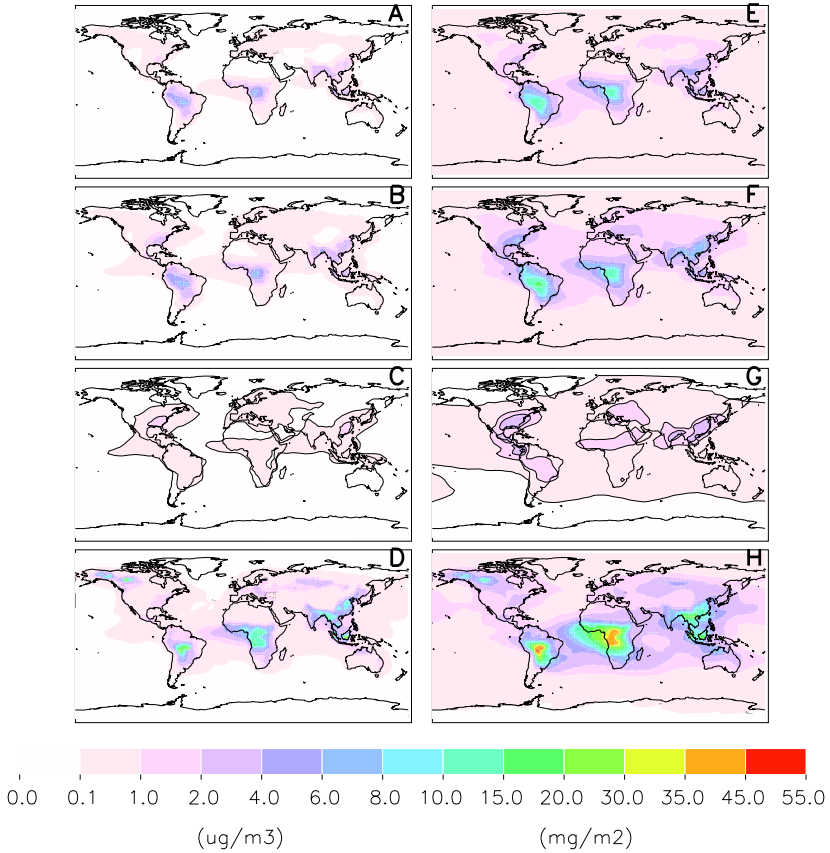

Fig. 1. Annual mean plots of SOA at the surface from runs R_1 and R_{sulf} (panels **(A)** and **(B)** respectively). Panel **(C)**: The increase in annual mean SOA concentration at the surface in R_{sulf} (i.e. $R_{sulf} - R_1$). Panel **(D)**: Annual mean primary organic aerosol at the surface. Panels **(E)**–**(H)**: as for (A)–(D), except values are for an integrated column.

ACPD
7, 9053–9092, 2007

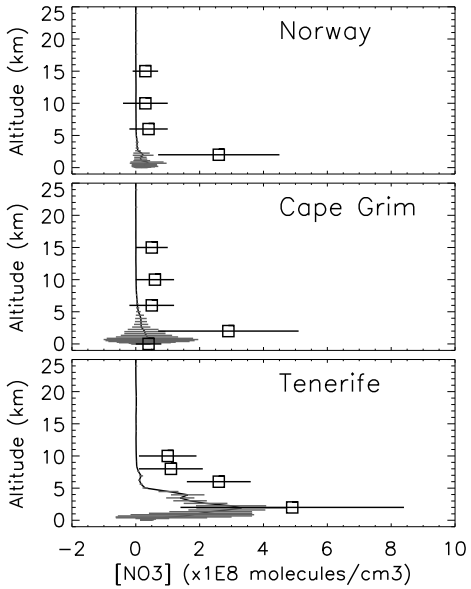

Fig. 2. Comparison of mean modelled NO_3 (solid line, with range of one standard deviation shown by horizontal grey bars) and measurements at three locations (squares, with range of one standard deviation shown by horizontal bars, from Allan et al. 2002).

ACPD
7, 9053–9092, 2007

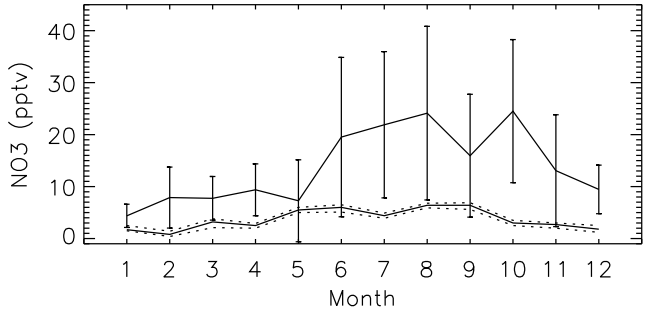

Fig. 3. Monthly mean nighttime modelled NO_3 mixing ratios (solid line, with vertical bars giving range of one standard deviation) and measurements made on Crete (lower line, with range of one standard deviation denoted by dotted lines, from Vrekoussis et al. 2006) between June 2001 and September 2003.

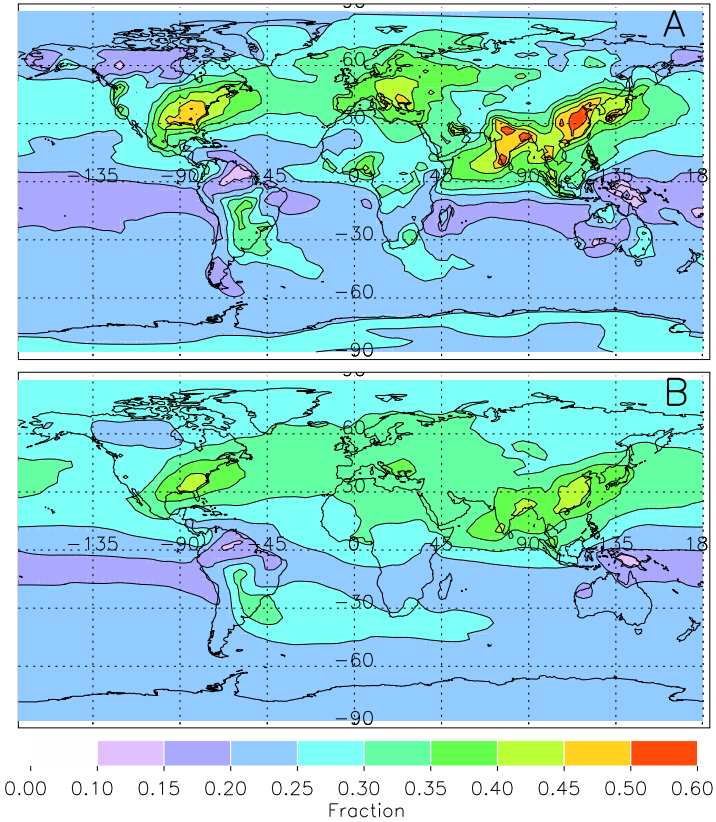

Fig. 4. The contribution of NO_3 oxidation to **(A)** surface SOA and **(B)** total column SOA.

ACPD
7, 9053–9092, 2007

EGU